

Nanostructured alumina from freeze-dried precursors

Regina Villanueva, Andrés Gómez, Pedro Burguete, Eduardo Martínez, Aurelio Beltrán, Fernando Sapiña

Institut de Ciència dels Materials, Parc Científic, Universitat de València

PO Box 22085, 46071 Valencia, Spain

Mónica Vicent, Enrique Sánchez

Instituto de Tecnología Cerámica - Asociación de Investigación de las Industrias Cerámicas

Universitat Jaume I, 12006 Castellón, Spain

Corresponding author: Fernando Sapiña

E-mail: fernando.sapina@uv.es

Abstract

Nanocrystalline alumina has been obtained on the 100-g scale by thermal decomposition of precursors resulting from the freeze-drying of aqueous solutions of different aluminium-containing products, namely aluminium acetate and aluminium L-lactate. Samples prepared at different temperatures (from 873 to 1573 K in steps of 100 K) were characterized by X-ray powder diffraction, scanning and transmission electron microscopy, and surface area measurements. In the acetate case, the transformation sequence involves the formation of θ -Al₂O₃ as an intermediate phase between γ - and α -Al₂O₃, whereas this θ phase is not observed in the lactate case. TEM and SEM images show the nanoparticulate character of the aluminas obtained at relatively low temperatures, with typical particle size in the 5 to 10 nm range. Progressive grain growth occurs as temperature increases. Otherwise, the precursor characteristics have a clear influence on the microstructure of the resulting aluminas, as reflected also by the measured BET surface area values. Whereas long aluminium acetate fibres results in open arrays of low aggregated alumina particles, large aluminium lactate sheets lead to comparatively compact alumina microstructures. Nanostructured alumina obtained from the lactate precursor has been reconstituted in a granulated powder with sufficient consistence and flowability to allow it to be thermal sprayed and deposited on a stainless steel substrate. X-ray powder diffraction data show that γ -Al₂O₃ is the major phase in the coating, which includes also α -Al₂O₃ particles. SEM results offer evidences on the nanostructured character of the coating.

Introduction

There is an increasing awareness of the potential of nanostructured coatings, both for replacing present coatings, due to their superior properties in comparison with their conventional (microstructured) counterparts, and for generating new applications.^{1,2} Studies have centred on ceramic-metal composites (cermets of the WC-Co type) and ceramic oxides.³⁻⁷ The reason for this choice is based on the particular characteristics of ceramic materials, such as high hardness and high thermal and corrosion resistance, which provide many advantages compared to polymers and metals when it comes to use as coatings, especially in applications in which wear, temperature, and corrosion resistance are simultaneously required.

Although several methods have already been used to date to prepare nanostructured coatings (sputtering, sol-gel...), the process that is most likely to find industrial implementation in the short term is thermal spraying and, in particular, plasma spraying, owing to its great versatility.⁸ In plasma thermal spraying (atmospheric plasma spraying being the most widespread method), the nanostructured starting powder is heated in a high-temperature gas stream to a semi-fused state, while concurrently being accelerated towards the substrate to be coated.⁹⁻¹⁴ When this material impacts the substrate, small lens-like deposits form (known as 'splats'), approximately 20 μm in diameter and 5 μm thick, from the semi-fused state. These splats solidify quickly at cooling rates of approximately 100 K/s. Coatings with thicknesses up to 200-300 μm can be produced by increasing the number of spray gun passes. Since this is a rapid process, in which the residence times during which the materials are exposed to high temperatures are extremely short, it might favour holding the nanostructure of the starting powder in the coating. In fact, progress of feedstock-particles melting (a process that has been thoroughly studied) depends on both plasma spraying conditions and the very nature of the feedstock.¹⁵⁻¹⁷ Thus, the maintenance of the starting powder nanostructure should be practically guaranteed in non melted zones. We will return on this point later on.

Under this approach, the seemingly obvious requirement for obtaining nanostructured coatings is to have at our disposal the adequate nanostructured starting powder. Nanostructured materials are ultrafine grained solids with a high proportion of atoms at grain boundaries. The key factor for industrial exploitation of nanostructured materials lies in the development of cost-effective, large scale manufacturing processes.^{18, 19} At present, more than two dozen different processes for their preparation have been described. However, most

of these methods are expensive, require sophisticated equipment, and yield relatively low production rates. Therefore, they have high production costs and are conceived for obtaining high value-added materials, with typical applications in the fields of electronics and photonics. In other cases, difficulties may appear owing to operation details. Indeed, a problem frequently associated with sol-gel related methods lies in the stoichiometric control and the cation distribution in multicomponent systems.

In this context, powder processing methods for the preparation of submicron and nanostructured powders in a controlled form, with a wide range of compositions, sizes and morphologies, need to be improved. The freeze-drying method was first successfully applied by E. W. Flosdorf in 1935 in the instant coffee industry. Nowadays this method is applied in the production of numerous advanced materials.²⁰⁻³³ The method consists of: a) fast freezing of a sprayed solution, b) vacuum drying by sublimation of the solvent, and c) decomposition of the resulting precursor to give rise to oxides, nitrides, or carbides by heat treatment in a controlled atmosphere. In comparison with other chemical methods, one of the advantages of this technique is its capacity to prepare polycrystalline powders with controlled characteristics. The commercial applications (electronics, pharmacy, catalysis, pigments, etc.) are determined by the specific properties of the resulting materials. As far as other competing synthesis processes are concerned, the disadvantages of the sol-gel method (difficult control of the stoichiometry and cation distribution in multicomponent systems) have been noted above. In the spray-drying method, on the other hand, the equipment has a high volume and a low production rate.

Alumina and mixtures of alumina and titania are used as coatings that withstand severe high temperature, friction, or corrosion environments.³⁴⁻³⁶ The present paper reports on how the use of freeze-dried precursors allows the preparation of nanostructured alumina powders at the 100-g scale. The nanostructured alumina was reconstituted in a granulated powder with sufficient consistency and flowability to allow it to be sprayed and deposited on stainless steel substrates.

Experimental

Synthesis

Materials. The materials used as reagents in this study were aluminium hydroxide, $\text{Al}(\text{OH})_3$ (Kemira Ibérica, 100%), aluminium L-lactate, $\text{Al}(\text{CH}_3\text{CHOHCOO})_3$ (Aldrich, 97.0%), cerium (III) acetate hydrate, $\text{Ce}(\text{CH}_3\text{COO})_3 \cdot 1.5\text{H}_2\text{O}$ (Aldrich, 99.9% pure), glacial acetic acid (Panreac 99.5%), and acetic anhydride (Panreac 98%).

Preparation of precursors. Aluminium hydroxide was transformed in a soluble acetate complex by refluxing for 24 h a suspension containing $\text{Al}(\text{OH})_3$ (0.7 mol) in a 1:1 (v:v) mixture of glacial acetic acid and acetic anhydride (50 mL). Then, the suspension was filtered and the resulting solid was washed with acetone. The precursor solution was prepared by refluxing for 3 h a suspension of the acetate complex (0.024 mol) in water (200 mL), what resulted in a clean solution whose concentration in Al^{3+} was 0.12 M.

Aluminium L-lactate precursor solution (0.60 M in Al^{3+}) was directly prepared by dissolving the salt (0.15 mol) in water (250 mL) under continuous stirring at room temperature. We also prepared a second precursor solution in which a small amount of cerium was present ($\text{Ce}^{3+}:\text{Al}^{3+}=1:100$ mol; $[\text{Al}^{3+}]=0.60$ M). Addition of cerium has the purpose of avoiding the carbon deposition observed on the products resulting from thermal decomposition of the cerium-free precursor at low temperatures. Cerium was handled as cerium (III) acetate, and was dissolved in the aluminium L-lactate solution. On the other hand, for considering possible effects on the microstructure of the final alumina associated to the concentration of the precursor solution, we prepared also analogous solutions whose concentration in Al^{3+} was 0.12 M. In order to improve efficiency for further treatments, we should have using precursor solutions as concentrated as solubility allow.

Droplets of these solutions were flash frozen by spraying on liquid nitrogen and, then, freeze-dried at a pressure of 10^{-4} atm in a Telstar Cryodos freeze-drier. In this way, dried solid precursors were obtained as amorphous (X-ray diffraction) loose powders. The thermal evolution of the precursors was monitored by thermogravimetric experiments (TGA-DTA) under oxygen atmosphere (heating rate 5 K min^{-1} , flow rate $50 \text{ cm}^3 \text{ min}^{-1}$), using a Setaram Setsys 16/18 system.

Synthesis of nanostructured alumina. Nanostructured alumina samples were synthesized by thermal decomposition of the amorphous precursor solids. A sample of the selected precursor was placed into

an alumina boat and introduced in the furnace. Several runs under different experimental conditions were performed in order to determine its influence on the structure and microstructure of the samples. The precursor powder was heated at 5 K min^{-1} to a final temperature T_f ($T_f = 573$ to 1573 K , in steps of 100 K) that was held for a period of time t_{hold} of 6 h under flowing oxygen. The solid was then cooled by leaving the sample inside the furnace (slow cooling, *ca.* 2 K min^{-1}). All products were stored in a desiccator over CaCl_2 .

Preparation of an alumina coating from nanostructured powder.

Feed powders. In most thermal spray methods, coatings are obtained from feedstock in powder form. As a result, in order to obtain nanostructured coatings by these techniques, it is convenient to use nanoparticles as raw material. However, nanoparticles cannot be sprayed directly owing to their low mass: they must be agglomerated to form micrometric particles. This process, which is critical for the success of the method, is known as reconstitution process. In fact, agglomerate size and density are critical for coating quality. The powder must be dense enough and have an appropriate particle size distribution. Fine and porous powders cannot be fed into the centre of the plasma flame. Indeed, they will float on the flame surface or will be evaporated by superheating before spattering on the substrate, what results in poor deposition efficiency and poor coating-bond strength.

Nanostructured alumina agglomerates with good cohesion and sufficient mechanical strength were prepared by forcing the granular association of precursor particles. With this aim, an aqueous solution (10 wt\%) of polyvinyl alcohol (PVA, MOWIOL 4/88 from Clariant) was used. A sample of the nanostructured alumina powder was deposited on a tray and sprayed with the PVA solution. It was then transferred to a granulating drum which was rotated at 200 rpm for 10 min . The amount of PVA added was *ca.* 1.0 wt\% (referred to powder sample). The resulting granulated powder was screened between 40 and $100 \mu\text{m}$. Finally, in order to enhance powder flowability, fumed silica (AEROSIL 200 from Evonik) was added to the granulated powder, and this mixture was again rotated in the drum for 10 min . The amount of fumed silica added was *ca.* 0.6 wt\% (referred to powder sample).

Coating processing by atmospheric plasma spraying. Atmospheric plasma spray (APS) is one of the most important and versatile techniques currently used by various sectors of industry for the deposition of wear-resistant ceramic coatings. During the process, the feedstock is injected in powder form inside the flame

at very high temperature (6000-12000 K). The powder is heated and accelerated until impact on the substrate surface, where it cools rapidly, forming the coating.

In this study, coatings were obtained by APS (Sulzer-Metco F4 MB plasma gun), mounted on an industrial robot (IRB1400 from ABB). Before spraying, the substrate was blasted with corundum grit and cleaned with ethanol to remove any dust or grease residue from the surface. The main spraying parameters were as follows: Ar flow rate, 35 slpm (standard litre per minute); H₂ flow rate, 12 slpm; arc intensity, 600 A, spraying velocity 1000 mm/s, and spraying distance 120 mm.

Characterization

Elemental analysis. Metal ratios in the cerium-containing samples were determined by energy-dispersive X-ray analysis (EDAX) on a scanning electron microscope (Hitachi S-4100, BSE AuTrata detector, EMIP 3.0 Software, and a RONTEC microanalysis system). Operating voltage was 20 kV, and the energy range of the analysis 0-20 keV. EDAX showed that the freeze-dried precursors were homogeneous at micron scale.

X-ray diffraction. X-ray powder diffraction patterns were obtained from a diffractometer using Cu-K_α radiation (Seifert XRD 3003 TT). Samples were dusted through a sieve on the holder surface. Routine patterns were collected with a scanning step of 0.08° at 2θ over the angular range 2θ 10–70° with a collection time of 5 s per step. All graphical representations relating to X-ray powder diffraction patterns were performed using adequate software (DRXWin Program).³⁷ This technique was also used to characterise the as-sprayed coating.

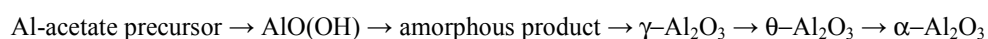
Microstructural characterization. The morphology of the freeze-dried precursors, the resulting oxides and the as-sprayed coating was observed using a scanning electron microscope-field emission (Hitachi 4100FE) operating at an accelerating voltage of 30 kV, and using also a transmission electron microscope (JEOL JEM 1010) operating at an accelerating voltage of 100 kV. All the SEM preparations were covered with a thin film of gold for better image definition.

Surface areas. The BET surface areas of the products were determined by nitrogen adsorption at 77 K, assuming a cross-sectional area of 0.162 nm² for the nitrogen molecule (Micromeritics ASAP 2000). Prior to adsorption measurements, the samples were outgassed in vacuum at 423 K for 18 h.

Results

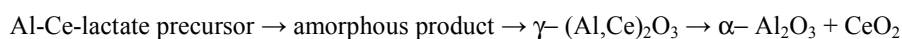
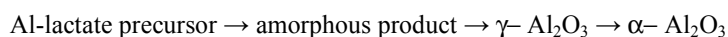
The thermal evolution of the precursors was monitored by TGA and X-ray powder diffractometry. Figure 1 shows the TGA curves corresponding to the thermal evolution under oxygen atmosphere (heating rate 5 K/min, flow rate 50 cm³/min) of the different freeze-dried powder precursors. In all cases, the onset of the thermal decomposition of the organic component of the precursor complexes occurs at *ca.* 475 K, and decomposition is complete at 675-700 K. Prior to this process (i.e., from room temperature until *ca.* 475 K), a relatively small (3-12 wt%) and continuous weight loss is observed for all samples, which could be associated to evolution of water molecules retained in the precursors. After water removal, decomposition of the precursors occurs in at least two-step superimposed processes.

Figure 2 shows the X-ray powder diffraction patterns of the products resulting from thermal treatment of the precursors at temperatures ranging from 1073 to 1473 K. The thermal treatments were performed under dynamic oxygen atmosphere for 6 h. In the case of the Al acetate samples, the presence of aluminium oxyhydroxide was observed at 573 and 673 K. By rising the treatment temperatures, it appeared firstly (773 K) an amorphous product, whereas transition aluminas were detected from 873 to 1273 K. Concerning these transition aluminas, γ -Al₂O₃ is the only crystalline product between 873 and 1073 K, while θ -Al₂O₃ is observed at 1173 and 1273 K. Although θ -Al₂O₃ remains as the major phase at 1373 K, we can now observe also weak peaks attributable to α -Al₂O₃. The α -Al₂O₃ phase becomes the major one at 1473 K, but the presence of θ -Al₂O₃ originates some weak peaks. Finally, at 1573 K, α -Al₂O₃ is the only detectable phase. Thus, the transformation sequence in the thermal decomposition of the acetate precursor can be written as follows:



Otherwise, dealing with the Al lactate samples, the final products from thermal treatments ranging from 573 to 973 K were amorphous. Crystallization of the γ -Al₂O₃ phase can be observed at 1073 K. Formation of α -

Al_2O_3 is not detected (as minor phase) until 1273 K. Finally $\alpha\text{-Al}_2\text{O}_3$ appears as the only crystalline phase at 1373 K and higher temperatures. In the case of Al-Ce lactate samples, the transformation sequence is similar to that described for the lactate precursor exempt from Ce. However, the appearance of $\alpha\text{-Al}_2\text{O}_3$ occurs at higher temperatures. In fact, both $\alpha\text{-Al}_2\text{O}_3$ and transition $\gamma\text{-Al}_2\text{O}_3$ phase peaks are observed at 1373 K. It is interesting to note that the CeO_2 peaks are not detected at relatively low temperatures (i.e. in the presence of $\gamma\text{-Al}_2\text{O}_3$). In fact, the CeO_2 peaks are not observed prior to the formation of some $\alpha\text{-Al}_2\text{O}_3$ (1373 K). These two facts suggest that a) $\gamma\text{-Al}_2\text{O}_3$ is able to form a solid solution that incorporates Ce(IV) ions, b) the presence of dissolved Ce(IV) ions stabilizes $\gamma\text{-Al}_2\text{O}_3$ with respect to $\alpha\text{-Al}_2\text{O}_3$, and c) the solubility limit of Ce(IV) in $\alpha\text{-Al}_2\text{O}_3$ is very low. Thus, the transformation sequences in the thermal decomposition of the lactate precursors are as follows:



The poor crystallinity of the low temperature polymorphs (γ and θ), as well as the influence on peak width of the disorder in the cation positions, prevents a clear picture of the temperature evolution of the crystallite size of these phases from being obtained. However, information was obtained on the $\alpha\text{-Al}_2\text{O}_3$ crystallite size. This size was calculated from XRD patterns by a standard Scherrer analysis of the half-width of the XRD peaks. LaB_6 from NIST (SRM660a) was used as standard to calibrate the intrinsic width associated with the equipment.³⁸ Crystallite sizes range, in all cases, from 70 to 200 nm, depending on the temperature and precursor. Thus, even at 1573 K, the $\alpha\text{-Al}_2\text{O}_3$ crystallites are very small.

Figures 3 to 5 show characteristic TEM and SEM images corresponding to some representative alumina samples. In the case of the Al acetate precursor, the freeze-dried powder is made up of fibres, several hundred nanometres long, with a diameter of about 5–10 nm. The external appearance of these fibres remains practically unchanged during the thermal decomposition process, as can be clearly observed in the micrograph of the sample prepared at 1073 K, Figure 3a. However, these fibres are now constituted by aggregates of nanometric particles with a typical size of 5–10 nm. At higher temperatures, a continuous small increase in

particle size is observed, together with a progressive collapse of the fibrillar microstructure. Between 1373 and 1573 K, Figure 3b, the collapse of the fibrillar array produces an open structure.

In the case of the Al lactate precursor, the evolution of the microstructure displays some differences. Indeed, the freeze-dried precursor consists of sheets with typical dimensions of 4000 x 4000 x 500 nm. Again, the external appearance of the precursor particles remains practically unchanged during relatively low temperature treatments (1073 K), as can be clearly observed in the micrograph shown in Figure 4a. A higher magnification image reveals that the product sheets consist of aggregates of nanoparticles with a typical size of 5-10 nm (Figure 4b). At higher temperatures, a certain increase in particle size is observed (Figure 4c). At 1573 K, strong grain growth and sintering is observed (Figure 4d).

Insofar as differences in precursor concentration salts (0.12 M for Al acetate and 0.60 M for Al lactate) could have some influence on the microstructural characteristics of the final products (because of effects due to the agglomeration degree after freeze-drying), we carried out comparative experiments starting from an aluminium L-lactate precursor solution 0.12 M in Al^{3+} . It must be stressed that neither X-ray patterns nor SEM micrographs corresponding to analogous products in these series (0.60 or 0.12 M Al lactate) reveal any noticeable difference. So, the observed differences in the behaviour of samples coming from aluminium acetate and aluminium L-lactate precursors should be related to the proper precursor nature, and not associated to concentration effects.

In the Al-Ce lactate case, the evolution of the microstructure is very similar to that of the Al lactate precursor: the large sheets of the original precursor are observed until 1373 K (Figure 5c), and consist of nanoparticle aggregates that grow slowly between 1073 and 1373 K (Figures 5a and 5b). At 1573 K, strong grain growth and sintering is observed (Figure 5d). However, there is a significant difference with respect to the Al lactate case: the presence in the surface of sintered grains of small particles with a typical size of about 80 nm. According to X-ray diffraction data, the presence of these small particles can be attributed to the segregation of CeO_2 during the $\gamma\text{-Al}_2\text{O}_3$ to $\alpha\text{-Al}_2\text{O}_3$ transformation.

These differences in the final microstructures, either open or more compact depending on the precursor, are clearly reflected in the evolution of the BET surface area of the samples (Figure 6). At a given

temperature, the BET surface area of alumina samples coming from the acetate precursor are significantly larger than those corresponding to lactate-derived samples.

Figure 7 shows the X-ray diffractogram of the coating prepared by using as feedstock nanostructured alumina obtained from the Al lactate precursor at 1073 K. As observed, γ -Al₂O₃ is the major phase in the coating but the presence of α -Al₂O₃ is evident. According to previous results in the literature, this is a usual situation: independent of the type of alumina used to apply the coating, the presence of mixtures of γ -Al₂O₃ and α -Al₂O₃ is always observed, the relative contents of both phases being mainly related to the sprayed aggregate size.^{39,40}

Figure 8 shows micrographs of the coating corresponding to both the outer layer (Figures 8a and 8b) and an inner surface as resulting from a transversal fracture (Figures 8c and 8d). As can be observed (Figure 8a), the porous as-sprayed surface exhibits an irregular topography. One can clearly appreciate the final image of the sprayed droplets (splats) together with zones in which comparatively small pseudofaceted particles prevail. Very likely, the as observed splats became deformed and partially disaggregated by hitting the substrate. When these splats are examined at higher magnification (Figure 8b), their surface appears as consisting of a highly compact array of nanoparticles. Otherwise, the surface generated after fracture shows the same microstructural features (splats and particle zones) than the outer layer (Figure 8c). Figure 8d shows a representative image, at high magnification, focused on a zone exempt from splats. As observed, the surface of the pseudofaceted particles also is composed of nanoparticles. By comparison with the splats case, these nanoparticles are higher and adopt a less compact disposition.

Discussion

It is well known that alumina crystallizes in many polymorphs⁴¹⁻⁴⁸ All these polymorphs can be classified into two groups, based on the arrangement of oxygen anions. There are structures based on a cubic compact packing (fcc), such as the γ , η , θ , or δ forms, or on a hexagonal compact packing (hcp), such as the α , κ , and χ forms. The differences between the polymorphs belonging to the same group are related to the arrangement of the cations in the holes of the compact packing of oxide anions. It is, thus, very difficult to differentiate among the polymorphs in each group. The different polymorphs are obtained by thermal

decomposition of a variety of precursors. Depending on the precursor (polymorphs of aluminium oxyhydroxide or hydroxide, for example), different Al_2O_3 structures are formed, which follow diverse sequences of phase transformations with increasing temperature. In all cases, the α form is the thermodynamically stable one at high temperatures under normal conditions. The detailed sequences and stability ranges have been attributed to many factors, such as crystallinity degree, presence of impurities, thermal history, among others.

Without prejudice to the above, there is abundant information in the literature supporting the idea that the alumina particle size has a great influence on the crystalline form adopted: nanoparticulate alumina crystallizes in the γ form and microparticulate alumina in the α form.⁴⁹ This is not an unique situation: nanoparticulate TiO_2 and ZrO_2 crystallize in anatase and tetragonal forms, respectively, and microparticulate TiO_2 and ZrO_2 in rutile and monoclinic forms, respectively.^{50, 51} Most researchers indicate that the microparticulate samples of these oxides adopt the thermodynamically stable structural variety, whereas those shown by nanoparticulate samples are metastable.⁵⁰ However, in 1993, molecular dynamic simulation of different γ and α - Al_2O_3 surfaces indicated that the surface energies of α - Al_2O_3 were significantly greater than those of γ - Al_2O_3 .⁵² These data suggested that γ - Al_2O_3 becomes the energetically stable polymorph of nanoparticulate alumina, as it was claimed by Navrotsky *et al.* in 1997.⁵³ Some months later, the group of Navrotsky reported experimental results showing that the surface energy of α - Al_2O_3 actually is significantly greater than that of γ - Al_2O_3 (2.64 versus 1.67 Jm^{-2} , respectively). As they concluded, this implies, in practice, that surface-energy differences thermodynamically stabilize nanoparticulate γ - Al_2O_3 over nanoparticulate α - Al_2O_3 .⁵⁴ Since then, this group has applied the same methodology, using high-temperature solution calorimetry data coupled with other techniques, to demonstrate that similar surface-energy differences also explain the TiO_2 , ZrO_2 and anhydrous and hydrated ferric oxides cases.⁵⁵⁻⁵⁷

Since the samples in this study are aggregated, we cannot obtain information on the surface area at which stability crossover occurs. Note, furthermore, that the aggregation state of the studied alumina samples depends on the precursor: it is low in the acetate case, and very high in the lactate case. Indeed, aluminas obtained from acetate, lactate and Ce-lactate- precursors have BET surface areas of 156, 21 and 41 m^2g^{-1} , respectively, at 1173 K. These differences in the aggregation state of the samples are in turn due to

differences in the microstructure of the original precursor: the fibrillar microstructure of the acetate precursors produces an open and poorly aggregated microstructure in the resulting aluminas, whereas the lamellar microstructure of lactate precursors produces a compactly aggregated microstructure. Owing to aggregation, it is clear that not all the surface is accessible for BET measurement. Thus, interfacial energies must contribute significantly to the total surface energy in the lactate derived samples, whereas their contribution must be relatively low in the acetate derived samples. Even more, the transformation sequence in the case of the acetate precursor includes the presence of θ - Al_2O_3 , whereas this phase is not observed in the transformation sequences of the lactate precursors. This strongly suggests that the presence of θ - Al_2O_3 can be attributed to a stabilization of this phase due to an energy crossover favoured at low aggregation degrees, but suppressed at high aggregation degrees.

Finally, some remarks need to be made concerning the coating characteristics. As noted above, although our powder feedstock was conformed by agglomeration of nanoparticulate γ - Al_2O_3 , the X-ray diffraction data show that the coating is built up from both γ - Al_2O_3 and α - Al_2O_3 . This is a systematic result concerning nanostructured alumina thermally sprayed coatings: independent of the structural variety used as feedstock, the resulting coating consists of mixtures of γ - Al_2O_3 and α - Al_2O_3 .^{39, 40} In the thermal plasma treatment, the nanoparticle agglomerates are subjected to very high temperatures. Depending on both the agglomerate features and plasma parameters, partial or total melting of the agglomerates occurs. Because of the high temperature conditions, the possible non fused (solid) regions in the generated droplets should mainly consists of particles of the stable α - Al_2O_3 . The short residence time does not make probable significant further particle growth by sintering. On hitting the substrate, quenching of the melt, at rates exceeding 100 K/s, leads to the formation of a great number of crystallization nuclei, which have low chance for growing. Thus, solidification (crystallization) of liquid droplets at considerable undercooling should result in the formation of γ - Al_2O_3 rather than α - Al_2O_3 , according to the stability crossover characterized by Navrotsky et al.⁵¹ The observed two-scale structure of the thermally sprayed coating (splats from molten regions of the agglomerates cementing retained solid particles) is what could be expected on a thermodynamic basis. In practice, this would make unnecessary kinetic ad hoc arguments to explain the presence of γ - Al_2O_3 .

when $\alpha\text{-Al}_2\text{O}_3$ is used as feedstock.⁴¹ In any case, the key role played by the feedstock powder microstructure features in determining the coating microstructure and thermo mechanical properties, make necessary further studies in order to adjust spray parameters for improving coating performances.¹⁶

Conclusion

In summary, alumina can be successfully prepared as nanoparticles on the 100-g scale by thermal decomposition at relatively low temperatures of precursors obtained by freeze-drying solutions of aluminium-acetate or aluminium L-lactate. The formation process shows that $\theta\text{-Al}_2\text{O}_3$ is produced as an intermediate phase in the acetate case, whereas this phase is not observed in the lactate case. The authors attribute this fact to the different aggregation state of the alumina particles, which depends on the microstructure of the corresponding precursor. A Ce-containing lactate precursor was also prepared in order to avoid the deposition of residual carbon in the course of the precursor decomposition at low temperature. Whereas Ce seems to be dissolved in $\gamma\text{-Al}_2\text{O}_3$, cerium oxide is clearly observed once $\alpha\text{-Al}_2\text{O}_3$ has formed. Finally, nanostructured alumina obtained from lactate precursor calcined at 1073K has been reconstituted into a granulated powder with sufficient consistency and flowability to allow it to be sprayed and deposited on a stainless steel substrates. Thermal sprayed coating partly retains the nanostructured character of the alumina powder.

Acknowledgements. This study has been supported by the Spanish Ministry of Science and Technology and EU FEDER Program (MAT2006-12945-C0-01, MAT2006-12945-C0-03, MAT2009-14144-C03-01, MAT2009-14144-C03-03). The SCSIE of the Universitat de València is gratefully thanked for the use of the X-ray diffraction, electron microscopy, and analytical facilities.

References

- ¹A. D. H. Cavaleiro and T. Jeff, "Nanostructured Coatings". Springer. New York (2006).
- ²S. C. Tjong and H. Chen, "Nanocrystalline materials and coatings," *Mater. Sci. Eng. R*, **44**, 1-88 (2004).
- ³J. H. He and J. M. Schoenung, "Nanostructured coating," *Mater. Sci. Eng. A*, **336**, 274-319 (2002).
- ⁴M. D. Salvador, J. J. Candel, V. Bonache, F. Segovia, V. Amigo, E. Sanchez and V. Cantavella, "Comportamiento a desgaste de recubrimientos de WC proyectados por plasma a partir de polvos micro y nanoestructurados," *Revista de Metalurgia*, **44**, 222-232 (2008).
- ⁵Y. Wang, W. Tian and Y. Yang, "Thermal shock behavior of nanostructured and conventional Al₂O₃/13 wt% TiO₂ coatings fabricated by plasma spraying," *Surf. Coat. Technol.*, **201**, 7746-7754 (2007).
- ⁶J. H. He and J. M. Schoenung, "A review on nanostructured WC-Co coatings," *Surf. Coat. Technol.*, **157**, 72-79 (2002).
- ⁷E. H. Jordan, M. Gell, Y. H. Sohn, D. Goberman, L. Shaw, S. Jiang, M. Wang, T.D. Xiao, Y. Wang, and P. Strutt, "Fabrication and evaluation of plasma sprayed nanostructured alumina-titania coatings with superior properties," *Mater. Sci. Eng. A*, **301**, 80-89 (2001).
- ⁸X. L. Jiang, C. B. Liu and F. Lin, "Overview on the Development of Nanostructured Thermal Barrier Coatings," *J. Mat. Sci. Technol.*, **23**, 449-456 (2007).
- ⁹F. L. Trifa, G. Montavon and C. Coddet, "On the relationships between the geometric processing parameters of APS and the Al₂O₃-TiO₂ deposit shapes," *Surf. Coat. Technol.*, **195**, 54-69 (2005).
- ¹⁰S. Guessasma and C. Coddet, "Microstructure of APS alumina-titania coatings analysed using artificial neural network," *Acta Mater.*, **52** [17], 5157-5164 (2004).
- ¹¹S. Guessasma and M. Bounazef, "Experimental design to study the effect of APS process parameters on friction behavior of alumina-titania coatings," *Adv. Eng. Mater.*, **6**, 907-910 (2004).
- ¹²H. Choi and C. Lee, "Responses of an atmospheric plasma sprayed (APS) alumina-titania coating to scratch wear," *J. Ceram. Process. Res.*, **5**, 214-222 (2004).
- ¹³M. Bounazef, S. Guessasma, G. Montavon and C. Coddet, "Effect of APS process parameters on wear behaviour of alumina-titania coatings," *Mater. Lett.*, **58**, 2451-2455 (2004).

- ¹⁴ H. Choi, C. Lee and H. Kim, "Effects of the plasma gas composition on the coating formation and coating properties of the APS Al₂O₃-TiO₂ coating," *J. Ceram. Process.*, **3**, 210-215 (2002).
- ¹⁵ Lima and B.R. Marple, "Thermal spray coatings engineered from nanostructured ceramic agglomerated powders for structural, thermal barrier and biomedical applications: a review," *J. Therm. Spray Technol.*, **16**, 40-62 (2007).
- ¹⁶ P. Fauchais, G. Montavon and G. Bertrand, "From powders to thermally sprayed coatings," *J. Therm. Spray Technol.*, **19**, 56-80 (2010).
- ¹⁷ M. Gell, E. H. Jordan, Y. H. Sohn, D. Goberman, L. Shaw and T. D. Xiao, "Development and implementation of plasma sprayed nanostructured ceramic coatings," *Surf. Coat. Technol.*, **146-147**, 48-54 (2001).
- ¹⁸ C. C. Koch, "Nanostructured materials: Processing, Properties and Applications," 2nd edition, Taylor & Francis, Norwich (2006).
- ¹⁹ C. N. R. Rao, "The chemistry of nanomaterials: Synthesis, Properties and Applications," Achim Müller, Anthony K. Cheetham ed.; Wiley-VCH, Weinheim (2004)
- ²⁰ G. Chen and W. Wang, "Role of Freeze Drying in Nanotechnology," *Drying Technol.*, **25**, 29-35 (2007).
- ²¹ C. Tallon, R. Moreno and M. I. Nieto, "Synthesis of γ -Al₂O₃ nanopowders by freeze-drying," *Mater. Res. Bull.*, **41**, 1520-1529 (2006).
- ²² W. M. Zeng, A. A. Rabelo and R. Tomasi, "Synthesis of α -Al₂O₃ Nanopowder by sol-freeze drying method," *Adv. Powder Technol.*, **189**, 16-20 (2001).
- ²³ N. Nikolic, L. Mancic, Z. Marinkovic, O. Milosevic and M. M. Ristic, "Preparation of fine oxide ceramic powders by freeze-drying," *Ann. Chim.- Sci. Mat.*, **26**, 35-41 (2001).
- ²⁴ O. A. Shlyakhtin, Y.-J. Oh and Y. D. Tretyakov, "Preparation of dense La_{0.7}Ca_{0.3}MnO₃ ceramics from freeze-dried precursors," *J. Eur. Ceram. Soc.*, **20**, 2047-2054 (2000).
- ²⁵ Y. D. Tretyakov, N. N. Oleynikov and O. A. Shlyakhtin, "Cryochemical Technology of Advanced Materials," Chapman & Hall Ltd., (1997).

- ²⁶ Y. Ng-Lee, F. Sapiña, E. Martínez-Tamayo, J. V. Folgado, R. Ibañez, F. Lloret and A. Segura, "Low-temperature synthesis, structure and magnetoresistance of submicrometric $\text{La}_{1-x}\text{K}_x\text{MnO}_{3+\delta}$ perovskites," *J. Mater. Chem.*, **7**, 1905-1909 (1997).
- ²⁷ T. Boix, Z. El Fadli, F. Sapiña, E. Martínez, A. Beltran, J. Vergara, R. J. Ortega and K. V. Rao, "Electronic Properties of Mixed Valence Manganates: the Role of the Cationic Vacancies," *Chem. Mater.*, **10**, 1569-1575 (1998).
- ²⁸ Z. El Fadli, E. Coret, F. Sapiña, E. Martínez, A. Beltran and D. Beltran, "Low temperature synthesis, structure and magnetic properties of $\text{La}_{0.85}(\text{Na}_{1-x}\text{K}_x)_{0.15}\text{MnO}_3$ perovskites: the role of A cation size disparity in the electronic properties of mixed-valence manganates," *J. Mater. Chem.*, **9**, 1793-1799 (1999).
- ²⁹ A. El-Himri, M. Cairols, S. Alconchel, F. Sapiña, R. Ibañez, D. Beltran and A. Beltran, "Freeze-dried precursor-based synthesis of new vanadium-molybdenum oxynitrides," *J. Mater. Chem.*, **9**, 3167-3171 (1999).
- ³⁰ A. El-Himri, F. Sapiña, R. Ibañez and A. Beltran, "Synthesis of new vanadium-chromium and chromium-molybdenum oxynitrides by direct ammonolysis of freeze-dried precursors," *J. Mater. Chem.*, **10**, 2537-2541 (2000).
- ³¹ A. El-Himri, F. Sapiña, R. Ibañez and A. Beltran, " $\text{Pd}_2\text{Mo}_3\text{N}$: a new molybdenum bimetallic interstitial nitride," *J. Mater. Chem.*, **11**, 2311-2314 (2001).
- ³² R. X. Valenzuela, G. Bueno, A. Solbes, F. Sapiña, E. Martínez and V. Cortés-Corberán, "Nanostructured ceria-based catalysts for oxydehydrogenation of ethane with CO_2 ," *Topics in Catalysis*, **15**, 181-188 (2001).
- ³³ D. Vie, N. Valero, E. Martínez, F. Sapiña, J. V. Folgado and A. Beltran, "A new approach to the synthesis of intermetallic compounds: mild synthesis of submicrometric Co_xM_y ($\text{M} = \text{Mo}, \text{W}$; $x : y = 3 : 1$ and $7 : 6$) particles by direct reduction of freeze-dried precursors," *J. Mater. Chem.*, **12**, 1017-1021 (2002).
- ³⁴ J. Zang, J. He, Y. Dong, X. Li and D. Yan, "Microstructure characteristics of Al_2O_3 -13 wt.% TiO_2 coating plasma spray deposited with nanocrystalline powders," *J. Mater. Process. Technol.*, **197** [1-3], 31-35 (2008).
- ³⁵ J. Zang, J. He, Y. Dong, X. Li and D. Yan, "Microstructure and properties of Al_2O_3 -13 % TiO_2 coatings sprayed using nanostructured powders," *Rare Met.*, **26**, 391-397 (2007).

- ³⁶ M. Gell, E. H. Jordan, Y. H. Sohn, D. Goberman, L. Shaw and T. D. Xiao, "Development and implementation of plasma sprayed nanostructured ceramic coatings," *Surf. Coat. Technol.*, **146-147**, 48-54 (2001).
- ³⁷ V. Primo, *Powder Diffrac.*, **14**, 70 (1999).
- ³⁸ A. K. West, "*Solid State Chemistry and its Applications*," John Wiley and Sons, Chichester, U. K. (1984).
- ³⁹ R. McPherson, "On the formation of thermally sprayed alumina coatings," *J. Mater. Sci.*, **15**, 3141-3149 (1980).
- ⁴⁰ G. N. Heintze and S. Uematsu, "Preparation and structures of plasma-sprayed γ - and α -Al₂O₃ coatings," *Surface and Coating Technology*, **50**, 213-222 (1992).
- ⁴¹ I. Levin and D. J. Brandon, "Metastable Alumina Polymorphs: Crystal Structures and Transition Sequences," *J. Am. Ceram. Soc.*, **81**, 1995-2012 (1998).
- ⁴² C. Wolverton and K. C. Hass, "Phase stability and structure of spinel-based transition aluminas," *Phys. Rev. B*, **63**, [024102] 1-16 (2000).
- ⁴³ S.-H. Cai, N. Rashkeev, S. T. Pantelides and K. Sohlberg, "Phase transformation mechanism between γ - and θ -alumina," *Phys. Rev. B*, **67**, [224104] 1-10 (2003).
- ⁴⁴ G. Paglia, C. E. Buckley, A. L. Rohl, B. A. Hunter, R. D. Hart, J. V. Hanna and L. T. Byrne, "Tetragonal structure model for boehmite-derived γ -alumina," *Phys. Rev. B*, **68**, [144110] 1-11 (2003).
- ⁴⁵ G. Paglia, C. E. Buckley, A. L. Rohl, R. D. Hart, K. Winter, A. J. Studer, B. A. Hunter and J. V. Hanna, "Boehmite Derived γ -Alumina System. 1. Structural Evolution with Temperature, with the Identification and Structural Determination of a New Transition Phase, γ' -Alumina," *Chem. Mater.*, **16**, 220-236 (2004).
- ⁴⁶ G. Paglia, C. E. Buckley, T. J. Udovic, A. L. Rohl, F. Jones, C. F. Maitland and J. Connolly, "Boehmite-Derived γ -Alumina System. 2. Consideration of Hydrogen and Surface Effects," *Chem. Mater.*, **16**, 1914-1923 (2004).
- ⁴⁷ G. Paglia, A. L. Rohl, C. E. Buckley and J. D. Gale, "Determination of the structure of γ -alumina from interatomic potential and first-principles calculations: The requirement of significant numbers of nonspinel positions to achieve an accurate structural model," *Phys. Rev. B*, **71**, [224115] 1-16 (2005).

- ⁴⁸ S. V. Tsybulya and G. N. Kryukova, "Nanocrystalline transition aluminas: Nanostructure and features of x-ray powder diffraction patterns of low-temperature Al₂O₃ polymorphs," *Phys. Rev. B*, **77**, [024112] 1-13 (2008).
- ⁴⁹ P. Ayyub, V. R. Palkar, S. Chattopadhyay and M. Multani, "Effect of crystal size reduction on lattice symmetry and cooperative properties," *Phys. Rev. B*, **51**, 6135–6138 (1995).
- ⁵⁰ R. C. Garvie, "The Occurrence of Metastable Tetragonal Zirconia as a Crystallite Size Effect," *J. Phys. Chem.*, **69**, 1238-1243 (1965).
- ⁵¹ A. A. Gibb and J. F. Banfield, "Particle size effects on transformation kinetics and phase stability in nanocrystalline TiO₂," *American Mineralogist*, **82**, 717-728 (1997).
- ⁵² S. Blonski and S. H. Garofaini, "Molecular dynamics simulations of α -alumina and γ -alumina surfaces," *Surf. Sci.*, **295**, 263-274 (1993).
- ⁵³ J. M. McHale, A. Navrotsky and A. J. Perrotta, "Effects of Increased Surface Area and Chemisorbed H₂O on the Relative Stability of Nanocrystalline γ -Al₂O₃ and α -Al₂O₃," *J. Phys. Chem. B*, **101**, 603-613 (1997).
- ⁵⁴ J. M. McHale, A. Auroux, A. J. Perrotta and A. Navrotsky, "Surface Energies and Thermodynamic Phase Stability in Nanocrystalline Aluminas," *Science*, **277**, 788-791 (1997).
- ⁵⁵ M. R. Ranade, A. Navrotsky, H. Z. Zhang, J. F. Banfield, S. H. Elder, A. Zaban, P. H. Borse, S. K. Kulkarni, G. S. Doran and H. J. Whitfield, "Energetics of nanocrystalline TiO₂," *PNAS* **99** [suppl. 2], 6476-6481 (2002).
- ⁵⁶ M. W. Pitcher, S. V. Ushakov, A. Navrotsky, B. F. Woodfield, G. Li, J. Boerio-Goates and B. M. Tissue, "Energy crossovers in nanocrystalline zirconia," *J. Am. Ceram. Soc.*, **88**, 160-167 (2005).
- ⁵⁷ A. Navrotsky, L. Mazeina and J. Majzlan, "Size-Driven Structural and Thermodynamic Complexity in Iron Oxides," *Science*, **319**, 1635-1638 (2008).
- ⁵⁸ D. Zois, A. Lekatou, M. Vardavoulas, I. Panagiotopoulos and A. Vazdirvanidis, "A Comparative Microstructural Investigation of Nanostructured and Conventional Al₂O₃ Coatings Deposited by Plasma spraying," *Journal of thermal spray technology*, **17**, 887-894 (2008).

Figure Captions

Figure 1. Characteristic TGA curves corresponding to Al acetate (dotted line), Al lactate (solid line) and Al-Ce lactate (dashed line) freeze-dried precursors.

Figure 2. X-ray diffraction patterns of materials prepared by thermal decomposition in oxygen of: a) Al acetate freeze-dried precursor, b) Al lactate freeze-dried precursor and c) Al-Ce lactate freeze-dried precursor. The temperatures of the thermal treatment are 1073 to 1473 K, in 100 K intervals, from bottom to top, in all cases.

Figure 3. TEM and SEM images showing the microstructure of the materials obtained from Al acetate freeze-dried precursors: (a) 1073 K, TEM; (b) 1573 K, SEM. Scale bars correspond to 100 and 1000 nm, respectively.

Figure 4. SEM images showing the microstructure of the materials obtained from Al lactate freeze-dried precursors: (a) and (b) 1073 K; (c) 1273 K; (d) 1573 K. Scale bars correspond to 2.5 μm , 250, 250 y 700 nm, respectively.

Figure 5. SEM images showing the microstructure of the materials obtained from Al-Ce lactate freeze-dried precursors: (a) 1073 K, SEM; (b) and (c) 1373 K, SEM; (d) 1573 K, SEM. Scale bars correspond to 200, 300, 400 and 800 nm, respectively.

Figure 6. Evolution of the BET area with the preparation temperature of the samples. Closed circles, acetate precursor samples, open circles, lactate precursor samples, closed square, Ce-lactate precursor samples.

Figure 7. X-ray diffraction pattern of the plasma sprayed-coating.

Figure 8. SEM images showing the microstructure of the plasma-sprayed coating: a) and b) surface and c) and d) fracture views. Scale bars correspond to 200 nm, 20 μm , 200 nm and 20 μm , respectively.